Insulin Storage and Glucose Homeostasis in Mice Null for the Granule Zinc Transporter ZnT8 and Studies of the Type 2 Diabetes–Associated Variants

Tamara J. Nicolson,[1] Elisa A. Bellomo,[1] Nadeeja Wijesekara,[2] Merewyn K. Loder,[1] Jocelyn M. Baldwin,[3] Armen V. Gyulkhandanyan,[2] Vasilij Koshkin,[2] Andrei I. Tarasov,[1] Raffaella Carzaniga,[4] Katrin Kronenberger,[4] Tarvinder K. Taneja,[1] Gabriela da Silva Xavier,[1] Sarah Libert,[5] Philippe Froguel,[6,7] Raphael Scharfmann,[8] Volodymir Stetsyuk,[8] Philippe Ravassard,[9] Helen Parker,[10] Fiona M. Gribble,[10] Frank Reimann,[10] Robert Sladek,[11] Stephen J. Hughes,[12] Paul R.V. Johnson,[12] Myriam Masseboeuf,[13] Remy Burcelin,[13] Stephen A. Baldwin,[3] Ming Liu,[14] Roberto Lara-Lemus,[14] Peter Arvan,[14] Frans C. Schuit,[15] Michael B. Wheeler,[3] Fabrice Chimienti,[6] and Guy A. Rutter[1]

OBJECTIVE—Zinc ions are essential for the formation of hexameric insulin and hormone crystallization. A nonsynonymous single nucleotide polymorphism rs13266634 in the *SLC30A8* gene, encoding the secretory granule zinc transporter ZnT8, is associated with type 2 diabetes. We describe the effects of deleting the ZnT8 gene in mice and explore the action of the at-risk allele.

RESEARCH DESIGN AND METHODS—*Slc30a8* null mice were generated and backcrossed at least twice onto a C57BL/6J background. Glucose and insulin tolerance were measured by intraperitoneal injection or euglycemic clamp, respectively. Insulin secretion, electrophysiology, imaging, and the generation of adenoviruses encoding the low- (W325) or elevated- (R325) risk ZnT8 alleles were undertaken using standard protocols.

RESULTS—ZnT8$^{-/-}$ mice displayed age-, sex-, and diet-dependent abnormalities in glucose tolerance, insulin secretion, and body weight. Islets isolated from null mice had reduced granule zinc content and showed age-dependent changes in granule morphology, with markedly fewer dense cores but more rod-like crystals. Glucose-stimulated insulin secretion, granule fusion, and insulin crystal dissolution, assessed by total internal reflection fluorescence microscopy, were unchanged or enhanced in ZnT8$^{-/-}$ islets. Insulin processing was normal. Molecular modeling revealed that residue-325 was located at the interface between ZnT8 monomers. Correspondingly, the R325 variant displayed lower apparent Zn^{2+} transport activity than W325 ZnT8 by fluorescence-based assay.

CONCLUSIONS—ZnT8 is required for normal insulin crystallization and insulin release in vivo but not, remarkably, in vitro. Defects in the former processes in carriers of the R allele may increase type 2 diabetes risks. ***Diabetes*** **58:2070–2083, 2009**

Glucose and other secretagogues stimulate the release of insulin, costored in secretory granules with Zn^{2+} ions, from pancreatic islet β-cells (1,2). The presence of two Zn^{2+} ions, located at the center of the insulin hexamer and coordinated via HisB10 and GluB13 (3), is thought to be essential for both the normal processing and crystallization of insulin. Moreover, zinc coreleased with insulin (4) may play an important paracrine role in the control of glucagon secretion in some (5,6), if not all (7), mammalian species.

ZnT8 is a member of a family of ten zinc transporters (ZnT1–10; encoded by *SLC30A1–10*) thought to catalyze the extrusion of Zn^{2+} from the cell cytosol into the extracellular space or intracellular organelles (8,9). Whereas ZnT1 is ubiquitously expressed and present at the cell surface (10), the remaining family members are located on intracellular organelles: notably late endosomes (ZnT2) (11), Golgi (ZnT5–7) (12), lysosomes (10), and synaptic vesicles (13). The roles of ZnT9 and ZnT10 (14) remain to be established. On the other hand, zinc uptake is mediated by members of the ZiP family (8).

With the exceptions of ZnT8 and ZnT3 (present in specialized glutaminergic neurons) (15), most ZnT family members are expressed in the majority of mammalian tissues. By contrast, ZnT8 (*SLC30A8*) mRNA levels are 2–3 orders of magnitude higher in the islet than in all other tissues examined (16–18), with low levels being detected in thyroid and adrenal cortex (18). Consistent with this restricted expression pattern, ZnT8 has been shown to be a major autoantigen in type 1 diabetes (19). Moreover, recent genome-wide studies (20,21) have shown that a nonsynonymous single nucleotide polymorphism rs13266634

From the [1]Section of Cell Biology, Division of Medicine, Imperial College London, London, U.K.; the [2]Department of Physiology, University of Toronto, Toronto, Canada; the [3]Institute of Membrane and Systems Biology, University of Leeds, Leeds, U.K.; the [4]Electron Microscopy Centre, Imperial College London, London, U.K.; [5]Mellitech, Grenoble, France; the [6]Section of Genomic Medicine, Division of Medicine, Imperial College London, London, U.K.; the [7]Centre National de la Recherche Scientifique Unite Mixte de Recherche 8090, Institute of Biology, Lille, France; [8]INSERM U845, University Paris Descartes, Paris, France; the [9]Centre National de la Recherche Scientifique and Université Pierre et Marie Curie, Paris, France; the [10]Cambridge Institute for Medical Research, University of Cambridge, Cambridge, U.K.; the [11]Department of Human Genetics, McGill University, Montreal, Canada; [12]Nuffield Department of Surgery, University of Oxford, Oxfordshire, U.K.; the [13]Institut de Medecine Moleculaire de Rangueil, INSERM U858, IFR31, Toulouse III University, CHU Rangueil, Toulouse Cedex, Toulouse, France; the [14]Division of Metabolism, Endocrinology & Diabetes, University of Michigan Medical School, Ann Arbor, Michigan; and the [15]Gene Expression Unit, Department of Molecular Cell Biology, Katholieke Universiteit Leuven, Leuven, Belgium.

Corresponding author: Guy A. Rutter, g.rutter@imperial.ac.uk.

Received 15 April 2009 and accepted 2 June 2009.

Published ahead of print at http://diabetes.diabetesjournals.org on 19 June 2009. DOI: 10.2337/db09-0551.

T.J.N., E.A.B., N.W., M.K.L., and J.M.B. contributed equally to this study.

© 2009 by the American Diabetes Association. Readers may use this article as long as the work is properly cited, the use is educational and not for profit, and the work is not altered. See http://creativecommons.org/licenses/by-nc-nd/3.0/ for details.

The costs of publication of this article were defrayed in part by the payment of page charges. This article must therefore be hereby marked "advertisement" in accordance with 18 U.S.C. Section 1734 solely to indicate this fact.

in the *SLC30A8* gene, resulting in the replacement of tryptophan-325 with arginine, increases the risk of type 2 diabetes (OR 1.58) possibly by decreasing insulin secretion and/or proinsulin processing (22,23).

Despite its clear role in both major forms of diabetes, the molecular and cellular mechanisms through which ZnT8 controls β-cell function remain undefined. Furthermore, although ZnT8 overexpression stimulates insulin release from INS-1 β-cells (17), the importance of the endogenous transporter has so far not been examined by silencing or genetic ablation. We show that ZnT8 mediates zinc uptake into insulin granules and influences insulin storage and glucose homeostasis in vivo.

RESEARCH DESIGN AND METHODS

Generation of ZnT8$^{-/-}$ mice. The strategy used is described in RESULTS. Briefly, *Slc30a8* knockout (ZnT8$^{-/-}$) mice were generated by GenOway (Lyon, France). This involved the insertion of a *Lox*P site together with an FRT (Flippase Recognition Target) flanked neomycin selection cassette within intron 1 and a single distal *Lox*P within the upstream exon 1 containing the translation initiation codon.

After homologous recombination in SV129-derived ES cells at the *slc30a8*/ZnT8 locus and injection into C57BL/6J blastocytes, the resulting *flox*'d mice were mated with CMV-*Cre*–expressing C57BL/6J mice. These were backcrossed three times (Toronto) or twice (London, Grenoble) onto a C57BL6 background. Separate colonies were maintained on normal rat diet with the fat/protein/fiber following contents: London, Grenoble, 2.7/14.4/4.7%; Toronto, 5.0/18.0/5.0%. Animals were continuously interbred to provide all three genotypes. ZnT8$^{-/-}$ mice were viable and obtained with the expected Mendelian frequency. Comparisons were made between sex-matched littermates unless otherwise indicated.

Histology and immunohistochemistry. Mouse pancreata were extracted and fixed in 10% neutral balanced formalin (Sigma) at 4°C for 18 h before dehydration and wax embedding and processing to obtain 5-μm slices (Carleton's Histological Technique, Drury and Wallington). Nuclei and cytoplasm were stained with hematoxylin and eosin, respectively. Sections were labeled with anti-insulin (1:300 dilution, Secondary-Alexa 488 1:1,000) and antiglucagon (1:200 dilution, secondary-Alexa 568 1:1,000) and sealed using Vector Shield Antifade Hard Set reagent (Vector Laboratories).

Brightfield and combined fluorescence and darkfield images were captured using a Zeiss Axiovert 200 inverted microscope with 2.5× air objective and a 1,300 × 1,000 pixel digital camera. Single islets within the slices were analyzed by confocal microscopy using a Zeiss Axiovert-200 microscope with an Improvision/Nokigawa spinning disc system running Volocity 4.0 (Improvision, Coventry, U.K.) software (24).

Human pancreata, fixed in 10% (v/v) formalin, were embedded in paraffin and sectioned. Sections (4 μm thick) were processed for immunohistochemistry (25) and labeled using mouse anti-insulin (Sigma, 1:2000), mouse antiglucagon (Sigma, 1:2000), and rabbit anti-ZnT8 (Mellitech, 1:200) and revealed with fluorescein anti-rabbit and Texas-red anti-mouse secondary antibodies (Jackson Immunoresearch, 1:200). Images were captured using a fluorescence microscope (Leitz DMRB, Leica) and digitized using a cooled CCD (C7780, Hamamatsu).

Human islet isolation. Islets were isolated from cadaveric donors according to ref. 26.

Gene expression analysis: islet cell populations. α- and β-cell populations were extracted from transgenic mice expressing the yellow fluorescent protein derivative Venus as described (27) (see supplemental METHODS, available in an online appendix at http://diabetes.diabetesjournals.org/cgi/content/full/db09-0551/DC1).

Microarray analysis was performed as described in supplemental METHODS. Quantitative RT-PCR (qPCR) for ZnT and ZiP isoforms was performed using SYBR Green on a 7900HT RealTime PCR system (Applied Biosystems) using three separate cell preparations (28).

ZnT8$^{-/-}$ mice. Total islet RNA was isolated using TRIzol Reagent (Invitrogen, San Diego, CA) and treated with rDNase I (Ambion, Austin, TX). Isolated RNA (1 μg) was reverse transcribed using Moloney murine leukemia virus reverse transcriptase (Invitrogen). Details of qPCR primer design and reactions are given in supplemental METHODS. Data were normalized to mouse β-actin mRNA.

Intraperitoneal glucose tolerance test (IPGTT). Glucose tolerance was assessed by intraperitoneal glucose injection. Mice were fasted for 5–15 h, weighed, and glucose (1.5 g/kg unless otherwise stated) administered via intraperitoneal injection. Glucose in tail vein blood was measured using a Glucometer (Accu-Check).

Euglycemic clamp. Mice were anesthetized with isoflurane (Abbott) and an indwelling catheter installed into the femoral vein (29). Insulin sensitivity was assessed 4 days after surgery (30,31).

Plasmid generation. cDNAs encoding human R325- or W325-ZnT8 were subcloned using primers bearing c-*myc* tags from hZnT8 and hZnT8-R325W EGFP fusion protein constructs (16) into plasmid pIRES2-EGFP (Clontech) or pIRES2-dsRed2 (Invitrogen). cDNA encoding a CD38-EGFP chimaera was generated as described under supplemental METHODS.

Expression was analyzed in INS-1(832/13) β-cells transfected using Lipofectamine2000 (Invitrogen) according to the manufacturers' instructions. Cells were visualized on a Leica SP5 laser-scanning confocal microscope.

Adenovirus construction. ZnT8-c-*myc* tagged-EGFP constructs were ligated into pAdtrack-CMV at *Kpn*I and *Eco*RV sites. Adenoviruses were produced as described (32).

Islet isolation and measurement of hormone secretion and processing. Islets were aseptically isolated by collagenase digestion of mouse pancreas (7) and insulin (24) and glucagon (7) secretion measured in batch incubations. Insulin processing was assessed by pulse-chase labeling with ^{35}S-methionine (33).

Electrophysiology. Plasma membrane potential (V_m) and whole-cell K_{ATP} channel conductance (G_{KATP}) of β-cells were recorded in perforated patch configuration (34). Electrical capacitance (C_m) and Ca^{2+} current (I_{Ca}) through the plasma membrane of β-cells were recorded in standard whole-cell configuration (24). See supplemental METHODS for further details.

Total internal reflection fluorescence microscopy. Isolated mouse islets were dispersed and infected with adenovirus expressing neuropeptide Y (NPY)-Venus (100 MOI) (35) before imaging (24). Release was stimulated using 50 mmol/l KCl, 1 μmol/l forskolin, and 25 μmol/l isobutyl-methylxanthine. Fusion events were detected by eye, and the release kinetics, defined by measuring changes in fluorescence within a 5-pixel diameter circle, analyzed using Microsoft Excel and fitted where appropriate to a first-order decay curve using Origin 7.5 software (OriginLab, Northhampton, MA).

Measurements of intracellular free [Ca^{2+}]. Intracellular free Ca^{2+} concentration ($[Ca^{2+}]_i$) was measured at 37°C using Fura-Red (Invitrogen) as previously described (7,24).

Transmission electron microscopy. Isolated islets were fixed and analyzed as previously described (24).

RNA interference and measurement of intracellular free Zn^{2+}. MIN6 cells were transfected using Lipofectamine 2000 (Invitrogen) with scrambled siRNA or siRNA against ZnT8 (5′-CCGUCAUGAUCUUAAAAGAtt-3′) (Ambion) or cotransfected with mCherry subcloned into pcDNA3.1 plasmid (Invitrogen, a gift from Dr. H. Gaisano, Toronto) and ZnT8-R325 or -W325 p-IRES constructs. After 24–48 h, cells were processed by immunocytochemistry (see Fig. 8*A*) or loaded with 3 μmol/l FluoZin-3 AM or Zinquin for 50 min at 37°C, then incubated for 10 min without dye, in perifusion buffer containing (mM) 130 NaCl, 5 KCl, 2 $CaCl_2$, 1 $MgCl_2$, 5 $NaHCO_3$, 1 glucose, 10 HEPES, pH 7.4 equilibrated with 5% CO_2/95% O_2. Coverslips were then transferred to an open chamber and continuously perifused with 5 μmol/l $ZnSO_4$ in the presence of 1 mmol/l glucose at 37°C. Membrane-permeable zinc ionophore pyrithione and zinc chelator N,N,N′,N′ tetrakis-(2pyridylmethyl) ethylene diamine were used as controls. Cells were imaged with or without continuous perifusion at 36–37°C using an Olympus BX51W1 fluorescent microscope controlled with Image Master3 software (PTI, Lawrencewille, NJ) with a high-speed monochromator (PTI). FluoZin-3 emission was monitored using 485 nm excitation, 505 nm beam splitter, and 525 nm band-pass filter. Zinquin emission was monitored using 365 nm excitation, 375 nm beam splitter, and 385 nm long-pass filter.

Coimmunoprecipitation. HeLa cells transfected with hZnT8-V5 and ZnT8-EGFP were lysed 48 h posttransfection, and immunoprecipitation was performed with Dynabeads Protein G (Invitrogen) coated with anti-V5 (Clontech) or anti-EGFP (Invitrogen) antibodies.

Homology modeling. The W325 form of ZnT8 was modeled on the crystal structure of the *Escherichia coli* zinc transporter YiiP (PDB accession 2QFI; resolution 3.8Å) (36) using Modeler version 8.2 (37). Alignment of the ZnT8 and YiiP sequences, which exhibit only ~19% sequence identity, was aided by comparison of the patterns of residue conservation in closer mammalian and bacterial homologues of these proteins, respectively, using the program ConSeq (38,39). One hundred models were generated, and the five of lowest energy were further analyzed using MolProbity (40). Of these shown in Fig. 6*C* 93% had residues in the allowed regions of the Ramachandran plot (the corresponding figure for 2QFI was 80%). The R325 variant of ZnT8 was generated from the model in silico using PyMOL (DeLano, W.L. The PyMOL Molecular Graphics System, 2002, www.pymol.org), which was also used to create the images shown in Fig. 6*C*.

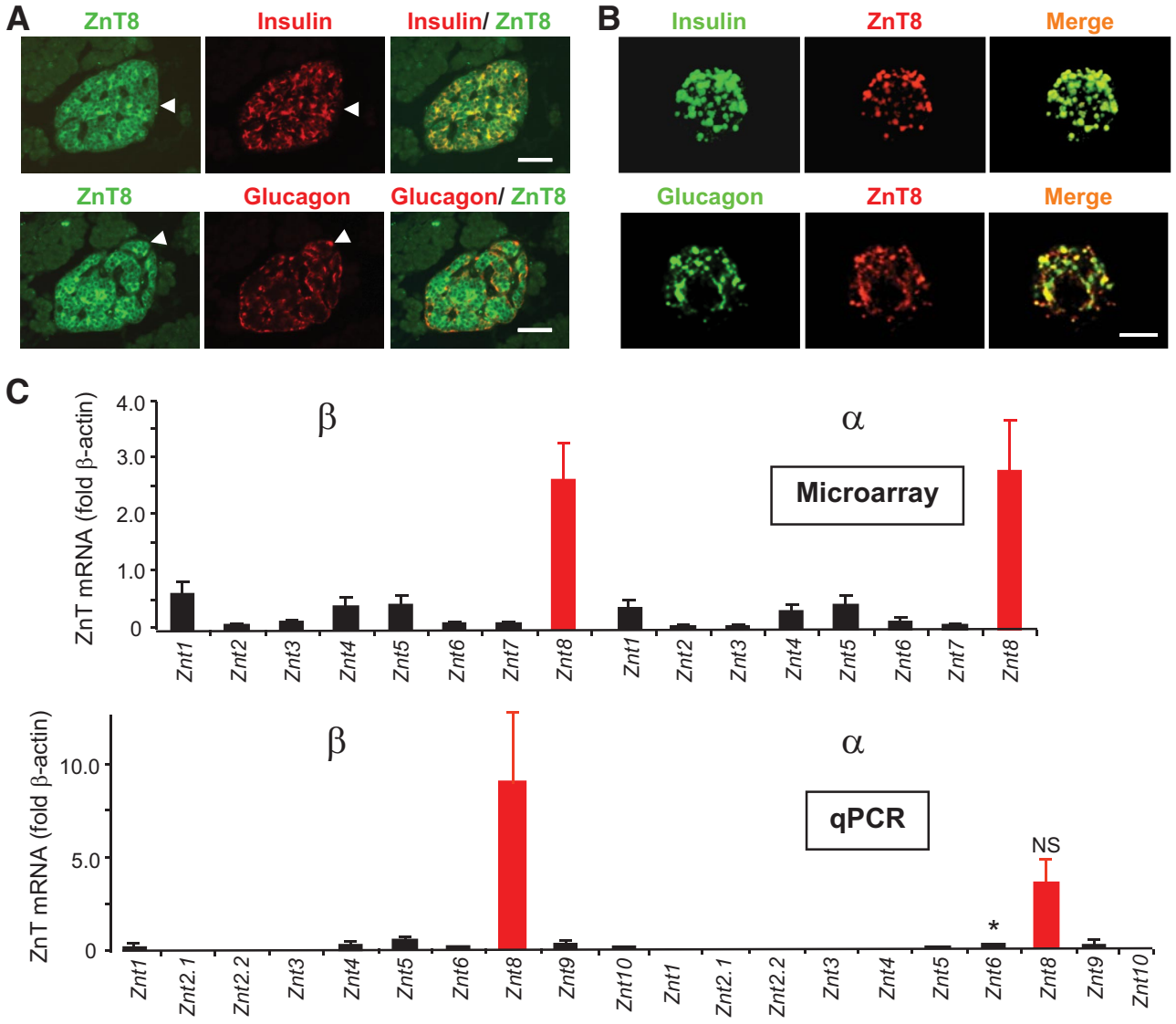

FIG. 1. Expression of ZnT8 in human pancreatic slices (*A*) and dissociated islet cells (*B*) and in purified wild-type mouse β- and α-cells (*C*). *A*: Pancreatic slices stained for ZnT8; scale bar, 50 μm. Cells in which clear colocalization to non–β-cells was apparent are highlighted with arrows. Essentially identical data were obtained with isolated human islets (not shown). *B*: Human islets were isolated (26) and dissociated with trypsin to allow the staining of single cells; scale bar, 5 μm. *C* and *D*: Mouse pancreatic α- and β-cells collected by flow cytometry from transgenic mice expressing the variant yellow fluorescent protein Venus under the control of the preproglucagon promoter (see supplementary METHODS). Three separate preparations of α- and β-cells were analyzed by either microarray analysis (*C*) or qPCR (*D*). *D*: Expression is presented relative to that of β-actin measured in the same sample. Primer and probe sequences are available on request. *$P < 0.05$ β- versus α-cell normalized mRNA levels. NS, not significant. (A high-quality digital representation of this figure is available in the online issue.)

Data analysis and statistics. Data were analyzed using Clampfit (Axon Instruments), CellR̂ (Olympus), and Excel (Microsoft) software. Statistical significance was estimated using Student's *t* test with appropriate Bonferroni correction. Pearson correlation statistics were analyzed with Simple PCI.

RESULTS

Expression of ZnT8 in the endocrine pancreas. ZnT8 immunoreactivity was localized to both β- and non–β-cells in isolated human pancreatic slices (Fig. 1*A*) and dispersed human islets (Fig. 1*B*) consistent with recent findings in rat pancreas (18). ZnT8 immunoreactivity was absent from neighboring acinar cells (Fig. 1*A*), in line with expression profiling (17,18). ZnT8 mRNA was absent in pancreata from neurogenin3-deleted ($ngn3^{-/-}$) mice, which lack an endocrine compartment, confirming restriction to the latter pancreatic cell types (supplementary Fig. 1 and see ref. 41). At the mRNA level, ZnT8 was the predominant ZnT family member in both FACS-purified α- and β-cells (Fig. 1*C*) (27), assessed by microarray (Affymetrix) analysis or quantitative PCR. Notably, in both purified β-and α-cells, ZnT8 mRNA levels exceeded by >10-fold the level of any other ZnT/*slc30a* family member (Fig. 1*C*).

Generation and histological examination of ZnT8$^{-/-}$ mice. To explore the potential in vivo role of ZnT8 we generated mice lacking the *slc30a8* gene. Deletion of exon 1 (Fig. 2*A* and *B*) led to essentially complete ablation of ZnT8 mRNA and protein expression (Fig. 2*C* and *D*) in isolated islets. No significant alterations were observed in the expression of other ZnT family members or the most abundant β-cell ZiPs (supplementary Fig. 2), ZiP6 or -7 (Fig. 2*D*). Examined at 12 weeks, β-cell mass was not significantly different between +/+ and −/− mice (Toronto colony: 3.1 ± 0.3 and 3.2 ± 0.2 islets/arbitrary area unit, respectively; London colony: 0.51 ±

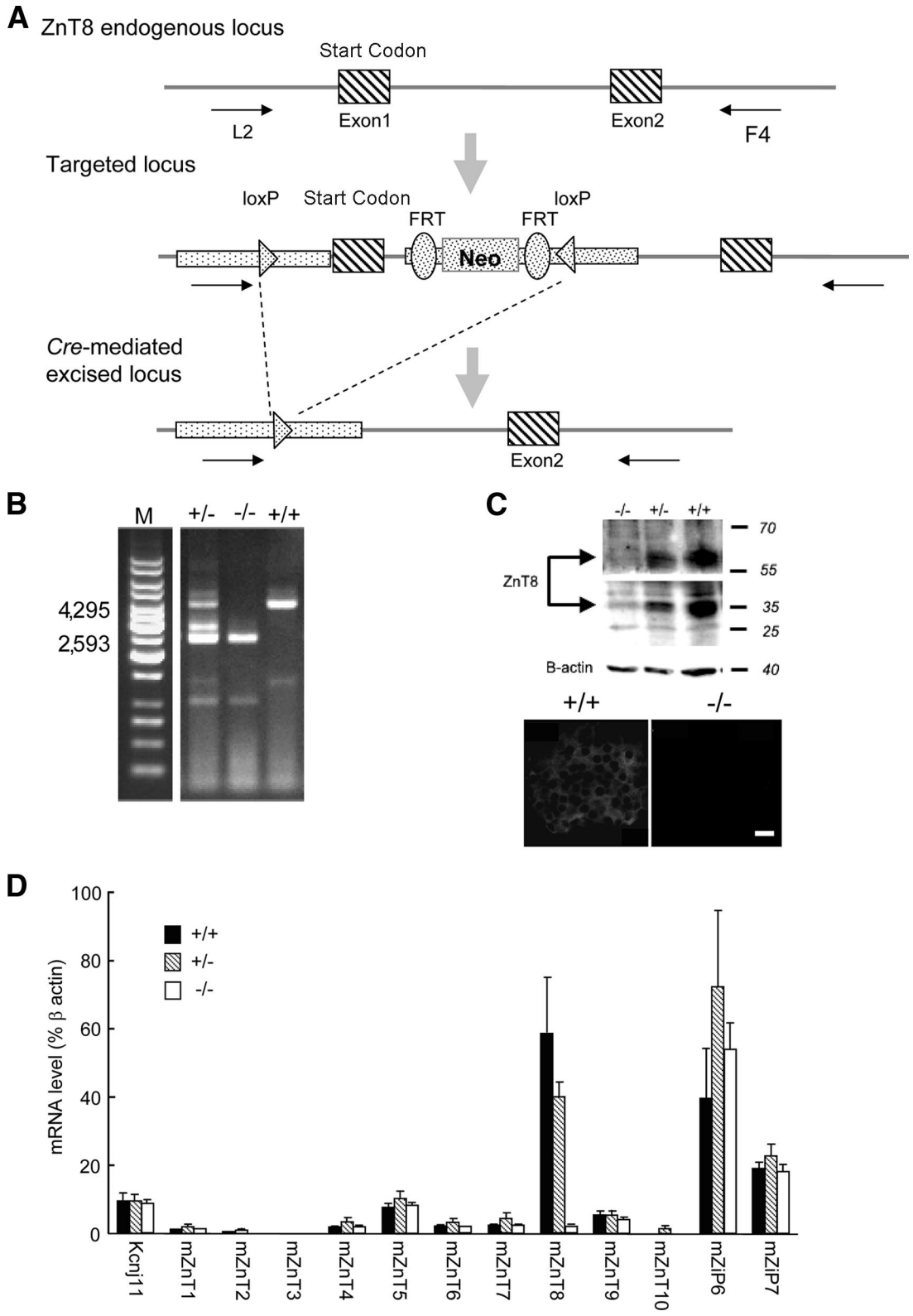

FIG. 2. Generation and genotyping of ZnT8$^{-/-}$ mice. *A*: See RESEARCH DESIGN AND METHODS for further details. *B*: Determination of genotype was performed on DNA tail biopsies by PCR amplification of genomic DNA using the following primers: L2: 5′-CTACTTCCATTTGTCACGTCCTG CACG-3′; F4: 5′-TGAAAACGGTGGGAAGCACTTGAGG-3′. The band migrating at ~4,000 (4,295 bp) corresponds to the endogenous locus (in the +/− case); the band at ~2,500 (2,593 bp) corresponds to the *Cre*-mediated excised locus. *C*: Western immunoblotting and immunocytochemical analysis of mice with the indicated phenotpyes. *D*: qPCR analysis of ZnT8 mRNA levels in islets from 8- to 12-week-old control and ZnT8$^{-/+}$ and $^{-/-}$ mice.

0.05 and 0.68 ± 0.03% total pancreatic surface; Fig. 3*A*). Moreover, the proportions of β- and α-cells did not differ between genotypes in either colony (Toronto: not shown; London, Fig. 3*B*). Surprisingly, normal insulin crystallization was not required to maintain unaltered insulin content in the absence of ZnT8 (for isolated

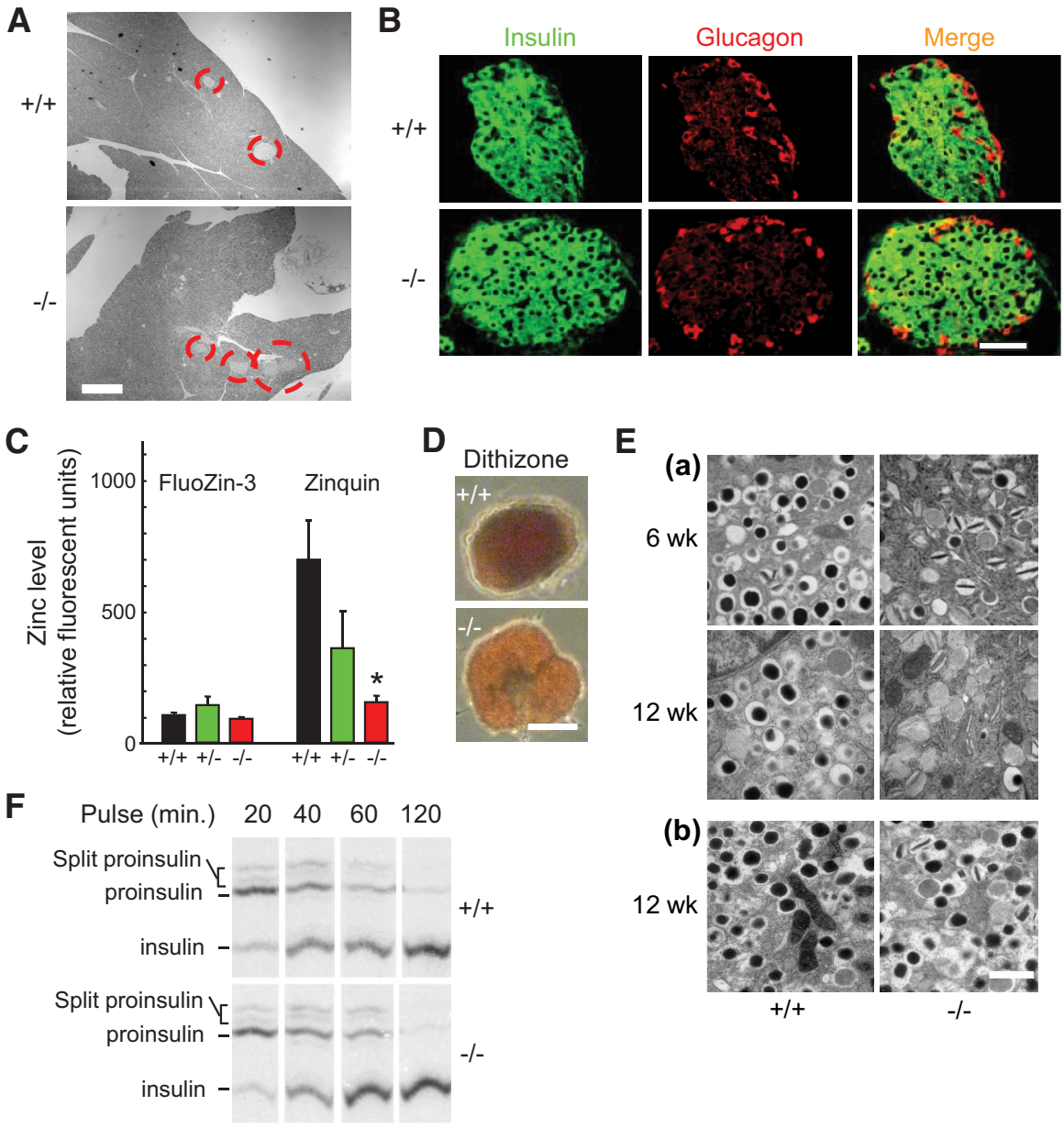

FIG. 3. Pancreatic histology, zinc accumulation, and insulin processing. *A*: Consecutive 5-μm pancreatic slices from 12-week-old wild-type or ZnT8$^{-/-}$ mice (London) stained by hematoxylin-eosin (Magnification ×2.5); islets are circled in red. *B*: Confocal images of pancreatic slices stained for insulin and glucagon (see RESEARCH DESIGN AND METHODS); scale bars, 50 μm. *C*: Intracellular zinc concentrations were estimated in isolated islets (Toronto) using FluoZin-3 (largely cytosolic; see Fig. 8*B*) or zinquin (granules; Fig. 8*B*). Fluorescence intensity per unit area was normalized by subtraction of the background average intensity in an area free of cells on the same coverslip, $n = 4–6$ islets per condition. *D*: Isolated islets (London) stained with 0.13 mmol/l dithizone for 5 min before imaging with a 5× objective on a Zeiss Axiovert 40 microscope; scale bar, 50 μm. *E*: Electron micrographs of isolated islets from ZnT8$^{-/-}$ animals and wild-type littermate controls at the indicated ages. Toronto (*a*) London (*b*) colonies; scale bar, 1 μm. *F*: Proinsulin conversion to insulin in the β-cells of islets isolated from ZnT8$^{-/-}$ or littermate control mice (12 weeks, London). (A high-quality digital representation of this figure is available in the online issue.)

size-matched 50- to 100-μm islets from London mice: 21.4 ± 5.8, 18.5 ± 5.7, and 13.7 ± 3 ng/islet for +/+, +/−, and −/−, respectively, $n = 5$ mice/genotype). Whereas zinc content measured with FluoZin-3 (mainly cytosolic; see below, Fig. 8*B*) was not reduced in ZnT8$^{-/-}$ mice (Fig. 3*C*), the zinc content of secretory granules and other organelles, estimated using zinquin (Fig. 3*C*) (42) or dithizone (Fig. 3*D*) (43) (Lemaire et al., unpublished data), was considerably (>70%) lowered in ZnT8$^{-/-}$ islets from either colony.

Examined by transmission electron microscopy, ZnT8$^{-/-}$ β-cells displayed a significantly larger number of granules lacking a detectable dense core and an increase in granules containing atypical, rod-shaped cores (Fig. 3*E*, supplementary Figs. 5–7), suggesting altered insulin crystal condensation (2). No difference in the number of granules morphologically docked at the plasma membrane was observed (supplementary Figs. 5*F* and 6*F*). The loss of dense core granules became more marked with age in Toronto mice (6 vs. 12 weeks; Fig. 3*E*; supplementary Figs. 5*C* and 6*C*). Proinsulin processing to split proinsulins and the mature hormone were unaltered in ZnT8$^{-/-}$ mice (London; Fig. 3*F*).

Glucose homeostasis and insulin secretion. Male ZnT8$^{-/-}$ mice maintained on normal rat diet displayed unaltered changes in body weight with respect to control

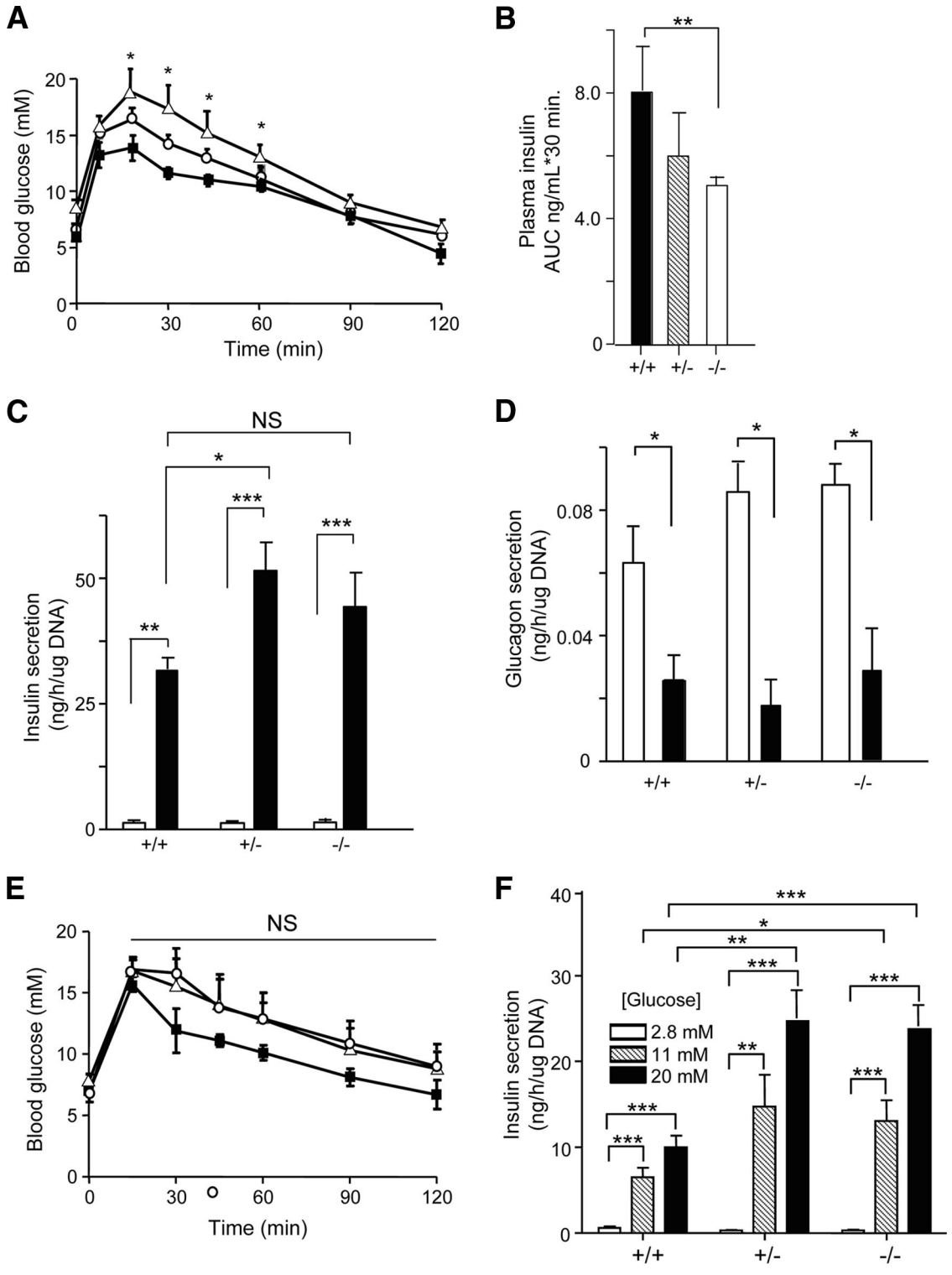

FIG. 4. Blood glucose homeostasis and insulin secretion in ZnT8$^{-/-}$ mice (Toronto) in (*A–D*) 6- and (*E* and *F*) 12-week-old mice. *A*: After a 5-h fast, glucose (1.5 g/kg) tolerance was assessed in 6-week-old male littermates. ■, +/+ (n = 12); ○, +/− (n = 8); ▲, −/− (n = 8). **P < 0.05 for the difference between wild-type and ZnT8$^{-/-}$ mice. *B*: Insulin levels were measured during IPGTT and the area under the curve (AUC) determined for each genotype. Secretion of insulin (*C*) and glucagon (*D*) from freshly isolated islets. Islets were from 3–12 separate mice per genotype. □, 0 mM glucose; ■, 20 mM glucose. *P < 0.05. *E* and *F*: Glucose tolerance (1.5 g/kg) assessed in 12-week-old mice as in *A*. NS, no significant difference in AUC for +/+ or +/− versus −/− mice. ■, +/+ (n = 6); ○, +/− (n = 3); ▲, −/− (n = 4). *F*: Glucose-stimulated insulin secretion assessed as in *A*(*c*). *P < 0.05, **P < 0.01, ***P < 0.001 for the indicated effects.

mice (London and Toronto colonies; not shown). In the Toronto colony, elevated fasting glucose levels and glucose intolerance during IPGTT were apparent in male ZnT8$^{-/-}$ mice at 6 but not 12 weeks (Fig. 4). Female ZnT8$^{-/-}$ mice in this colony displayed normal fasting glucose but were glucose intolerant at both ages (supplementary Fig. 4). Male null mice in the London colony were also glucose intolerant at both ages (supplementary Fig. 8) whereas normal glucose tolerance was seen in female null mice at 12 weeks (supplementary Fig. 8).

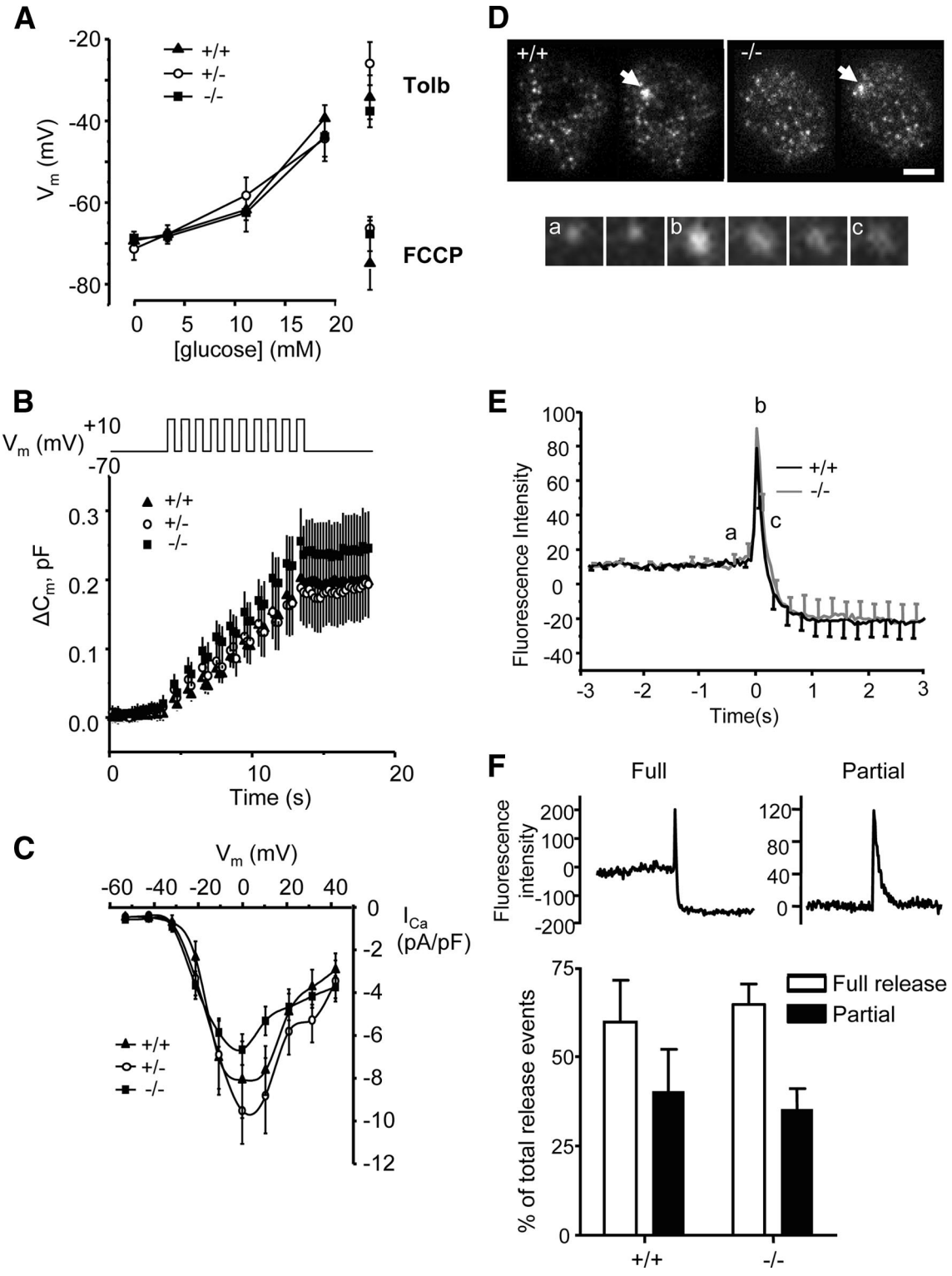

FIG. 5. Electrophysiological changes and TIRF imaging of exocytosis in single β-cells. *A*: Membrane potential, (*B*) depolarization-induced capacitance changes, and (*C*) Ca^{2+} currents recorded in pancreatic islet cells: $ZnT8^{+/+}$ (▲, $n = 17$), $ZnT8^{+/-}$ (○, $n = 16$), and $ZnT8^{-/-}$ (■, $n = 26$) animals (London, 12 weeks). *A*: Mean values of the whole cell capacitance change versus time are given; data were reduced to show 200 points for clarity. The stimulation protocol is given schematically above the graph. *D*: TIRF images of β-cells before and after stimulation; scale bar, 5 μm. Release events are indicated by an arrow. Snapshots of a single release event. *a–c*: Mark the points seen on the graph in *E* Kinetics of NPY Venus release. Data are normalized to baseline to exclude expression artifacts. Data expressed as the average of 38 versus 43 events (6 vs. 12 separate cells for +/+ vs. −/−; three separate preparations per genotype). *F*: Proportion of full and incomplete release events.

Whereas normal insulin sensitivity was observed in $ZnT8^{-/-}$ mice (Toronto, not shown; London, supplementary Fig. 9), in vivo insulin release under IPGTT was significantly reduced (Fig. 4*A*[*b*]). At 12 weeks, glucose-induced insulin secretion was significantly enhanced in $ZnT8^{-/-}$ mouse islets (Toronto; Fig. 4*A*[*c*] and *B*[*b*]),

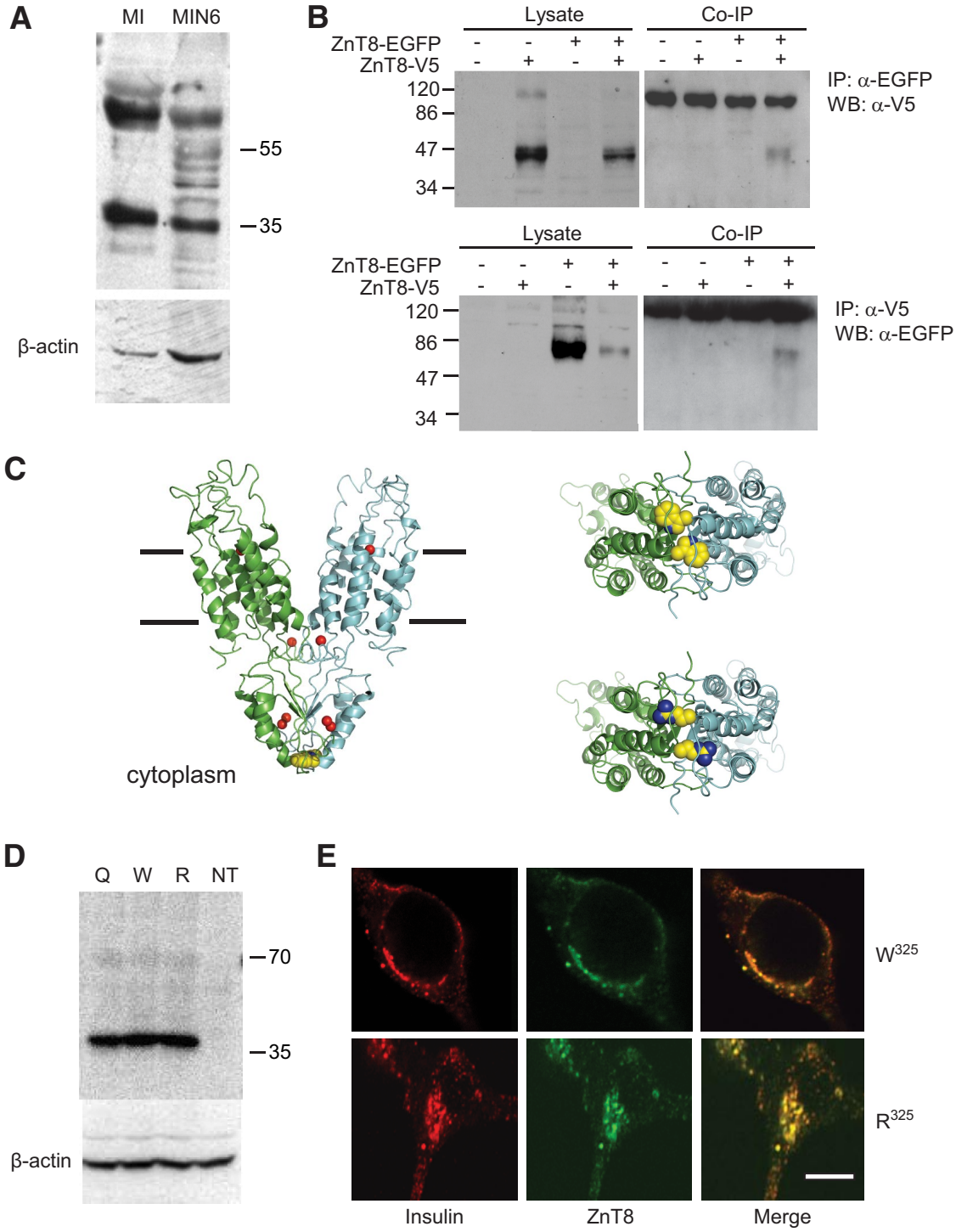

FIG. 6. Effect of R325W polymorphism rs13266634 on the predicted molecular structure of ZnT8 and on subcellular localization and stability. *A*: Western immunoblotting of ZnT8 in mouse islets and clonal MIN6 β-cells. Total lysates were separated by 10% SDS-PAGE and immunoblotted with anti-rat/mouse ZnT8 polyclonal antibodies (Mellitech, France) or anti–β-actin polyclonal antibody (43 kDa; Sigma). *B*: Dimer formation. Human ZnT8-V5 and ZnT8-EGFP were transfected into HeLa cells. Forty-eight hours posttransfection, cells were lysed and subjected to immunoprecipitation with antibodies against EGFP (*upper panel*) or V5 (*lower panel*) tags. After washing the beads, bound proteins were eluted and subjected to immunoblotting, probing with anti-V5 (*upper*; predicted molecular mass for ZnT8-V5, 46.4 kDa) or anti-EGFP (*lower*; predicted molecular mass for ZnT8-EGFP, 68.2 kDa) antibodies. "NS" denotes a nonspecific band, likely derived from IgG lost from the sepharose beads. *C*: Modeling of ZnT8 structure based on YiiP. The human transporter was modeled using the structure of the *Escherichia coli* transporter YiiP (PDB accession 2QFI) as a template. *Left, upper right*: Provide views of the W325 variant from the plane of the membrane and the cytoplasmic side of the membrane, respectively; *lower right*, view of R325 variant from cytoplasmic side of the membrane. The likely locations of zinc ions are shown as red spheres in *left*, and residues at position 325 are shown in space-filling representation in all panels. *D*: Western immunoblotting analysis of overexpressed ZnT8 isoforms in MIN6 cells. *E*: Subcellular distribution of overexpressed ZnT8 isoforms in INS-1(832/13) cells; scale bar, 5 μm. (A high-quality digital representation of this figure is available in the online issue.)

whereas glucose-inhibited glucagon secretion was unaffected (Fig. 4*A*[*d*]). In islets from the London colony examined at 12 weeks, basal insulin release was significantly enhanced ($ZnT8^{-/-}$ vs. wild-type) but glucose- or

KCl-induced secretion did not differ between genotypes (supplementary Fig. 8[*c*]).

Examined in the Toronto colony, a high-fat diet led unexpectedly to a greater gain in body weight in ZnT8$^{-/-}$ than wild-type mice (supplementary Fig. 3*A* and *C*). Under this regimen, null mice displayed elevated fasting blood glucose (supplementary Fig. 3*D*) and insulin (supplementary Fig. 3*F*) levels. Tendencies toward abnormal glucose tolerance, elevated glucagon levels, and decreased insulin sensitivity were also apparent (supplementary Figs. 3*B*, *E*, and *G*, respectively).

Effects of ZnT8 deletion on β-cell metabolism and exocytosis. Examined in single β-cells from 12-week-old male ZnT8$^{-/-}$ mice (London), no significant loss of glucose- or sulfonylurea-induced membrane depolarization (Fig. 5*A*) or ATP-sensitive K^+ (K_{ATP}) currents (not shown) were apparent, indicative of normal glucose metabolism. Similarly, depolarization-induced whole β-cell capacitance changes (Fig. 5*B*) and Ca^{2+} currents (Fig. 5*C*) remained unchanged, consistent with preserved exocytosis.

To determine whether the kinetics of granule cargo discharge may be affected by abnormal insulin crystallization, total internal reflection fluorescence (TIRF) analysis of release events was performed in single islet cells infected with adenovirus encoding neuropeptide-Y fused to the enhanced and red-shifted variant of green fluorescent protein, Venus (NPY-Venus) (Fig. 5*D–F*) (35). Exocytosis was stimulated by KCl in the presence of the cAMP-raising agents forskolin and isobutyl-methylxanthine. This protocol maximized the number of detectable events and ensured rapid fusion pore dilation, previously shown to lead to "full" events in which the entire granule cargo was released (44). In this way, crystal dissolution was expected to be rate limiting for the dispersal of the fluorescence after fusion. No differences were obtained in the rate of NPY-Venus diffusion ($t_{½}$ = 0.17 ± 0.02 s [+/+] vs. 0.17 ± 0.03 s [−/−]) suggesting that crystal dissolution was not affected by the absence of ZnT8 (Fig. 5*E* and *F*). Moreover, there was no difference in the number of "full" events, leading to complete or near complete loss of granule fluorescence (Fig. 5*E* and *F*), or "partial" release events in which granule fluorescence remained after the transient increase during fusion (Fig. 5*F*) (35).

Impact of type 2 diabetes polymorphisms on ZnT8 function. To assess the potential impact of replacement of the lower-risk with the higher-risk residue at position-325, we undertook homology modeling studies based on the bacterial zinc transporter and ZnT homologue, YiiP. A member of the cation diffusion facilitator transporter family (38), YiiP reportedly functions as a dimer (36), confirming similar behavior for mammalian ZnT8 from β-cell lines migrated on SDS-PAGE as bands with apparent molecular masses of ~40 and ~90 kDa and indicating the presence of monomers and possibly an SDS-resistant dimer (Fig. 6*A*) (18). To confirm the existence of dimers in living cells, we coexpressed EGFP- or V5-tagged ZnT8 in epithelial HeLa cells and performed immunoprecipitation experiments. Efficient coprecipitation indicated the existence of the transporter as dimers (Fig. 6*B*). Based on the structure of YiiP (36), the probable locations of Zn^{2+} ion binding sites in both the cytoplasmic and transmembrane domains of the ZnT8 model, the latter accessible from extracellular/intragranular side of the membrane, were inferred from the bacterial protein structure (Fig. 6*C*). Residue-325, at the cytoplasmic "tip" of each monomer in the homology model, forms part of the dimer interface and in different mammalian species is occupied by lower or higher risk (*Homo sapiens*), Q (rat and mouse), or higher risk (macaque) (supplementary Fig. 10). The impact of replacing lower with higher risk was assessed by in silico mutagenesis and revealed minimal distortion in overall folding (Fig. 6*C*). Although confirmation of the precise arrangement of this region of the protein awaits determination of the crystal structure, alignment of the ZnT8 sequence with the template structure in this region of the homology model was supported by analysis of the pattern of residue conservation (see RESEARCH DESIGN AND METHODS).

To identify potential physiological differences between β-cells expressing either the low-risk or increased-risk variants of ZnT8 we used plasmid-based transfection or adenovirus-mediated infection to introduce either form of the protein into β-cell lines. Each isoform displayed a similar expression level as evidenced by Western immunoblotting (Fig. 6*D*) and immunocytochemical analysis of single cells transfected with pIRES2-based plasmids (Fig. 6*E*). Moreover, close subcellular colocalization with insulin-containing granules, apparent for endogenous ZnT8 in human β-cells (Fig. 1*B*) (17), was also apparent for each of the overexpressed c-*myc*–tagged variants (Pearson correlation coefficient 0.77 ± 0.01 and 0.78 ± 0.02 for higher- and lower-risk mutants, respectively; Fig. 6*E*).

We next examined the effects of each ZnT8 allele on the regulation of insulin release. No significant differences in glucose-stimulated insulin secretion were apparent in INS-1(832/13) cells (Fig. 7*A*) or MIN6 β-cells (not shown) between cells overexpressing either the higher- or the lower-risk variant.

Measured in the whole-cell perforated-patch configuration, resting membrane potential (V_m) was identical in MIN6 cells overexpressing either vector alone, R325-ZnT8, or W325-ZnT8 (Fig. 7*B*), and the resting conductance of ATP-sensitive K^+ channels (G_{KATP}) was also of the same order in each case (Fig. 7*B*). No differences in glucose- or KCl-induced increases in apparent intracellular free Ca^{2+} ($[Ca^{2+}]_i$) were apparent between cells overexpressing R- or W325-ZnT8 (Fig. 7*C*). However, overexpression of either ZnT8 isoform significantly potentiated $[Ca^{2+}]_i$ increases in response to elevated glucose concentrations (Fig. 7*D*), suggestive of an effect of ZnT8 overexpression on either Ca^{2+} channel numbers or via changes in intracellular cation handling.

The effects of overexpression of either isoform on intracellular free Zn^{2+} concentrations ($[Zn^{2+}]_i$), were next explored using trappable intracellular Zn^{2+}-selective dyes: FluoZin-3, Zinquin ethyl-ester, or RhodZin3-AM (45). Whereas FluoZin-3 (Fig. 8*B*) and RhodZin-3 (not shown) were localized largely to the cytosol and nuclear compartments, Zinquin displayed marked punctate staining (Fig. 8*B*) (46), consistent with accumulation into secretory granules (47). We monitored zinc uptake by incubation in the presence of a supraphysiological concentration (5–10 μmol/l) of zinc ions. Suggesting that ZnT8 may mediate uptake of Zn^{2+} into the cytosol as well as the secretory granules, rates of uptake monitored with FluoZin-3 were diminished when the endogenous transporter was silenced (Fig. 8*A*). Initial rates of Zn^{2+} uptake were markedly elevated after overexpression of the W- but not the R325-ZnT8 variant as chimaeras with mCherry (Fig. 8*B*) consistent with a higher Zn^{2+} transporting activity of the former. In contrast to the c-*myc*–tagged chimaera (Fig. 6*E*), over-

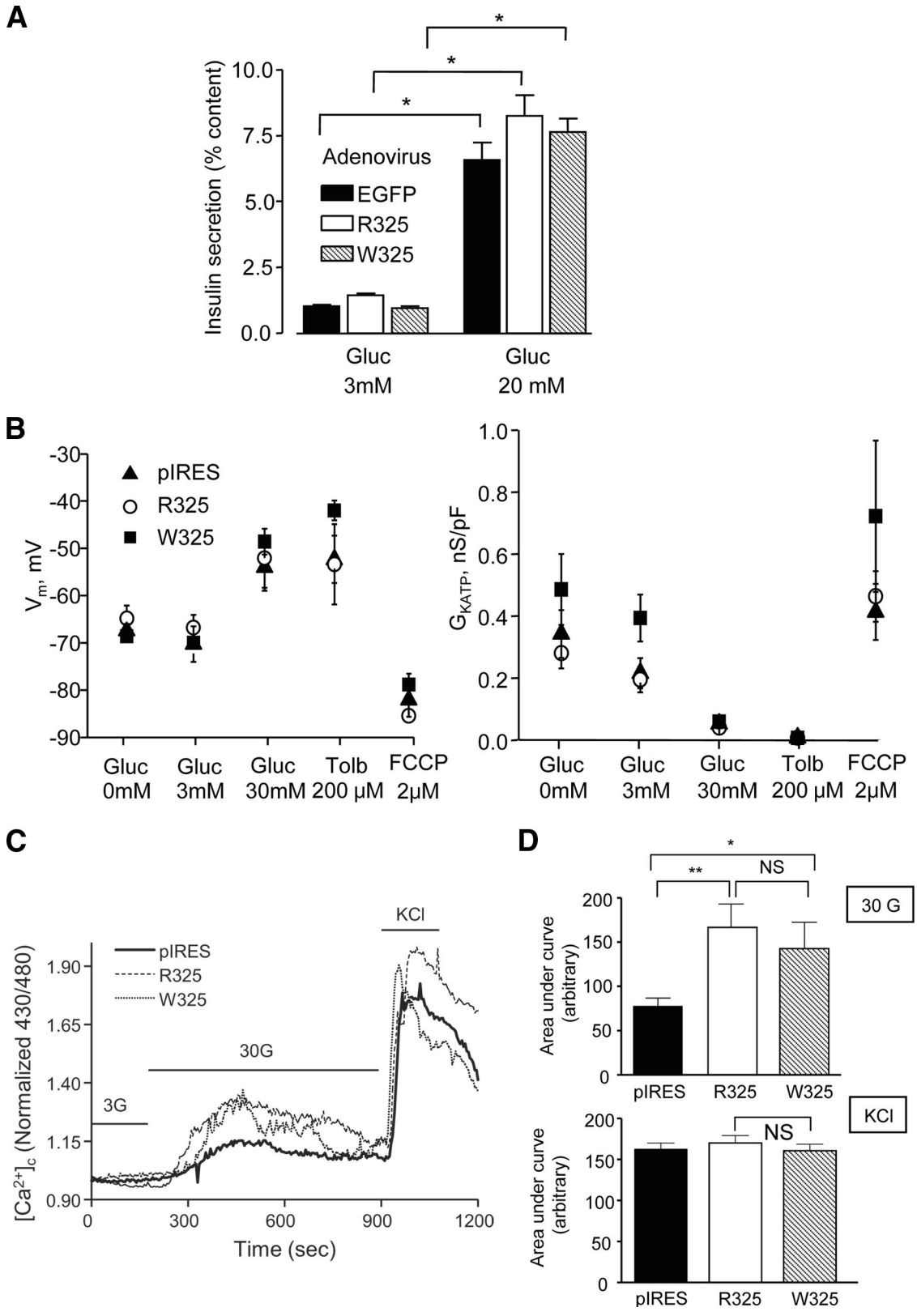

FIG. 7. Effects of R325W polymorphism of ZnT8 on insulin secretion and processing and on glucose signaling. *A*: INS-1(832/13) cells were infected with adenovirus encoding either EGFP only or the indicated ZnT8 isoform. Forty-eight hours later, cells were incubated for 30 min at the indicated glucose concentrations (n = 6 separate cultures from two independent experiments). *B*: Membrane potential and K_{ATP} channel conductance in MIN6 cells overexpressing the indicated ZnT8 isoform (n = 6 in each case) in pIRES2. *C*: Typical traces describing changes in intracellular free Ca^{2+} ($[Ca^{2+}]_i$) in individual MIN6 cells overexpressing the indicated ZnT8 isoform from plasmid pIRES2, or empty vector, and stimulated with the indicated concentrations of glucose or KCl (50 mmol/l). *D*: Combined data from responding cells in *C*. The graphs describe the increase in cytosolic $[Ca^{2+}]$ as AUC after stimulation with 30 mmol/l glucose (*upper panel*, CTRL n = 13, R325 and W325, n = 8 cells) or 50 mmol/l KCl (*lower panel*, CTRL n = 46, R325 n = 45, W325 n = 42). *$P < 0.05$, **$P < 0.01$ for the indicated effects.

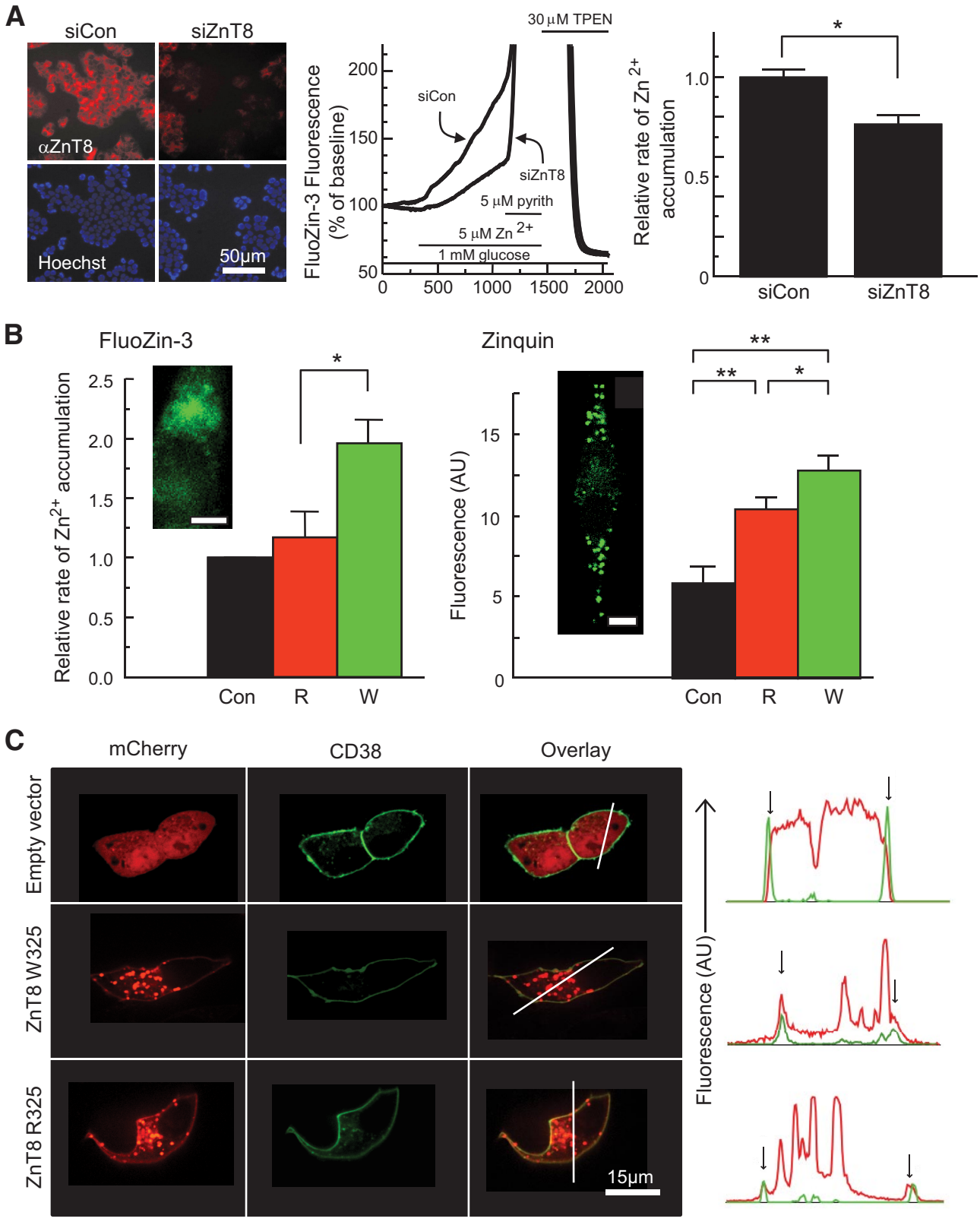

FIG. 8. Role of ZnT8 in cellular Zn^{2+} transport and effects of the R325W polymorphism. *A*: ZnT8 expression was reduced by RNAi as assessed by immunocytochemical analysis of cells fixed in 4% (v/v) paraformaldehyde and incubated with rabbit anti-mouse ZnT8 antibody (Mellitech, 1:3,000) and anti-rabbit–conjugated secondary antibody (1:500) plus Hoechst dye (5 μg/ml) before imaging on a Zeiss Axiovert inverted optics microscope. Zn^{2+} uptake into single MIN6 cells was assessed by monitoring changes in FluoZin-3 fluorescence (RESEARCH DESIGN AND METHODS). Under the conditions used in these experiments, the FluoZin-3 fluorescence increase gives an almost linear readout during the perifusion with $ZnSO_4$. The relative rates of Zn^{2+} accumulation were calculated from the slopes of the corresponding fluorescence changes. *$P < 0.05$ versus siCon, $n = 5$ independent experiments, 108–117 cells per condition. Calibrated resting free $[Zn^{2+}]_i$ was 600–700 pmol/l (NS, higher vs. lower risk). *B*: R325 or W325 ZnT8 were overexpressed in MIN6 cells, and transfected cells were identified by fluorescence of cotransfected mCherry-expressing vector before measurements of the initial rate of apparent Zn^{2+} uptake as in *A*. *$P < 0.05$ versus control or ZnT8-R, $n = 5$ independent experiments, 67–115 cells per condition. Zinc accumulation into granules was assessed using zinquin after incubation for 4 h in the presence of

expression of either variant interestingly led to detectable labeling of the plasma membrane as well as granules (Fig. 8*C*), suggesting that ZnT8 was able to mediate zinc transport across both membranes. Importantly, zinc accumulation into granules, assessed using zinquin (Fig. 8*B*), was significantly higher for overexpressed W- versus R-ZnT8.

DISCUSSION

Impact of ZnT8 deletion on insulin release. We show that ZnT8 is required for the normal accumulation of zinc by β-cell granules, for normal insulin crystallization and glucose tolerance. However, the impact of ZnT8 deletion appeared to depend subtly upon variations in genetic background, as well as age, sex, and diet. Unexpectedly, and for reasons that remain to be elucidated, we also show that ZnT8 is required for normal body weight homeostasis under metabolic (high-fat diet) stress. Whether human carriers of the at-risk R-allele are similarly affected is presently unknown.

Studied in male ZnT8$^{-/-}$ mice on a substantially C57BL6 background (Toronto colony; see RESEARCH DESIGN AND METHODS), glucose tolerance improved with age (from 6–12 weeks). Interestingly, this change was associated with a decrease (from 35–16%) in the number of dysmorphic, "rod-like" granules but an increase (from 24–36%) in electron-lucent ("empty") granules (Fig. 3*E*), whereas glucose tolerance normalized over the same period (Fig. 4). By contrast, in the London colony, rod-like still predominated over electron-luscent granules in ZnT8$^{-/-}$ mouse β-cells at 12 weeks: glucose-stimulated insulin secretion was not enhanced with respect to wild-type controls, and the mice remained glucose intolerant (supplementary Fig. 8). Such observations may suggest that a preponderance of atypical crystals, rather than their total absence, contributes to abnormalities in insulin release and hence glucose intolerance.

Surprisingly, we observed no abnormalities in insulin processing neither in ZnT8$^{-/-}$ islets from the London colony nor in islets from mice where dense cores were essentially eliminated (Lemaire et al., unpublished data) questioning the requirement of insulin crystallization for this process. Likewise, the kinetics of insulin release as assessed by TIRF microscopy were unchanged under conditions favoring the formation of large fusion pores (35). However, basal insulin release from ZnT8$^{-/-}$ islets was enhanced (supplementary Fig 8[*c*]), perhaps indicative of more efficient release of noncrystalline (mono/dimeric) insulin when fusion pores are small (35).

ZnT8 is expressed in α-cells. We show here that ZnT8 is expressed in the majority of α-cells in both humans and rodent islets. Nonetheless, no differences in the morphology of α-cell granules in ZnT8$^{-/-}$ mice were apparent (not shown). Moreover, we observed no alterations in the regulation by glucose of glucagon secretion from ZnT8$^{-/-}$ islets (Fig. 4*A*[*d*]), questioning the importance of zinc release from β-cells in the control of the latter process (7).

Activities of polymorphic variants of ZnT8. Although polymorphisms in the ZnT8/*SLC30A8* gene that alter the risk of type 2 diabetes (20,48) are likely to have a milder effect on glucose homeostasis than that of whole body inactivation of *slc30a8* in mice as described here, it seems likely they may alter β-cell Zn^{2+} content and hence the normal storage of insulin. We also confirm that this transporter is likely to be important for the uptake of Zn^{2+} into granules. However, the assay for ZnT8 transporter activity we have developed here unexpectedly revealed that the transporter may operate in the "reverse" direction, whereby low levels of ZnT8 on the plasma membrane also permit influx into the cell in the face of high Zn^{2+} concentrations. Similar bidirectional zinc transport has also been described for ZnT5 (49).

Importantly, we show here that the at-risk R-form of ZnT8 is less active as a zinc transporter. We also demonstrate by molecular modeling that R325 resides at the monomer interface, a site important for the transport activity of YiiP and other bacterial citation diffusion facilitator transporters (36,50). The resultant introduction of positive charge into this region of ZnT8, close to the predicted sites of bound structurally important Zn^{2+} ions, may be expected to affect the kinetics of Zn^{2+} transport and possibly the recruitment of zinc-metallochaperones (50). Carriers of this allele may therefore accumulate zinc, and thus package insulin, less efficiently into β-cell granules. Future studies, possibly using appropriately engineered mice expressing either allelic form of the transporter, will be needed to test this hypothesis.

The present report demonstrates that ZnT8 modulates glucose homeostasis in mice and shows that a "high risk" allele for type 2 diabetes displays decreased activity. Small molecule activators that target ZnT8 may thus represent an interesting new means to treat insulin secretory deficiency in this disease.

ACKNOWLEDGMENTS

G.A.R. thanks the Wellcome Trust (Programme Grant 081958/Z/07/Z), the Medical Research Council (G0401641), National Institutes of Health (ROI DK-O71962-01), and the European Union FP6 (SaveBeta) for grant support. F.M.G. and F.R. received Clinical and Basic Science Senior Fellowships, respectively, from the Wellcome Trust. E.A.B. and T.J.N. received Divisional Studentships from Imperial College. S.A.B. thanks the Biotechnology and Biological Sciences Research Council (Grant number BBS/B/14418) and the University of Leeds for support. F.C.S. was supported by Gene Ontology Annotation 2004/11 (K.U.Leuven, EURODIA LSHM-CT-2006-518153; European Community) and Juvenile Diabetes Research Fund Grant 1-2006-182. Work in the R.S. laboratory was supported by Institut National de la Sante et de la Recherche Medicale (INSERM) and the Association Française des Diabetiques (AFD). M.B.W. was funded by an operating grant from the Canadian Institutes of Health Research (CIHR, MOP-49521) and N.W. by a CIHR doctoral award. The work in the R.Sk. laboratory was funded by the Canadian Institutes for Health Research.

F.C. and S.L. are employed by Mellitech. No other potential conflicts of interest relevant to this article were reported.

We thank M.T. Gage-Soufflot for assistance with immunocytochemistry, Gao Sun, Nasret Harun, and Sahar Vak-

10 μmol/l $ZnSO_4$. Insets show the localization in single cells of FluoZin-3 and zinquin, as monitored by confocal microscopy. Note the punctuate distribution of zinquin, consistent with accumulation of the dye into secretory granules; scale bar, 5 μm. (*C*) Localization of overexpressed ZnT8-mCherry chimaeras at the plasma membrane, identified using CD38-EGFP. Note the presence of plasma membrane–associated ZnT8-mCherry fluorescence (red), coincident with CD38-EGFP (green) in the line plots (vertical arrows). (A high-quality digital representation of this figure is available in the online issue.)

shouri for able technical assistance. We thank Sabrina Mosaheb for preliminary electron microscopy experiments. We thank M. Nonnenmacher for technical expertise in coimmunoprecipitation experiments. We thank Christian Leibig and Martin Spitaler of the Facility for Live Cell Imaging and Microscopy (Sir Alexander Fleming Building, Imperial College London) and Lorraine Lawrence (NHLI) for valuable assistance with imaging and histology, respectively, and Sebastian Barg for advice on capacitance measurements.

REFERENCES

1. Rutter GA, Parton LE. The β-cell in type 2 diabetes and in obesity. Front Horm Res 2008;36:118–134
2. Dodson G, Steiner D. The role of assembly in insulin's biosynthesis. Curr Opin Struct Biol 1998;8:189–194
3. Baker EN, Blundell TL, Cutfield JF, Cutfield SM, Dodson EJ, Dodson GG, Hodgkin DM, Hubbard RE, Isaacs NW, Reynolds CD. The structure of 2Zn pig insulin crystals at 1.5 A resolution. Philos Trans R Soc Lond B Biol Sci 1998;319:369–456
4. Michael DJ, Ritzel RA, Haataja L, Chow RH. Pancreatic β-cells secrete insulin in fast- and slow-release forms. Diabetes 2006;55:600–607
5. Ishihara H, Maechler P, Gjinovci A, Herrera PL, Wollheim CB. Islet β-cell secretion determines glucagon release from neighbouring α-cells. Nat Cell Biol 2003;5:330–335
6. Zhou H, Zhang T, Harmon JS, Bryan J, Robertson RP. Zinc, not insulin, regulates the rat α-cell response to hypoglycemia in vivo. Diabetes 2007;56:1107–1112
7. Ravier MA, Rutter GA. Glucose or insulin, but not zinc ions, inhibit glucagon secretion from mouse pancreatic α-cells. Diabetes 2005;54:1789–1797
8. Devirgiliis C, Zalewski PD, Perozzi G, Murgia C. Zinc fluxes and zinc transporter genes in chronic diseases. Mutat Res 2007;622:84–93
9. Que EL, Domaille DW, Chang CJ. Metals in neurobiology: probing their chemistry and biology with molecular imaging. Chem Rev 2008;108:1517–1549
10. Falcon-Perez JM, Dell'Angelica EC. Zinc transporter 2 (SLC30A2) can suppress the vesicular zinc defect of adaptor protein 3-depleted fibroblasts by promoting zinc accumulation in lysosomes. Exp Cell Res 2007;313:1473–1483
11. Palmiter RD, Cole TB, Findley SD. ZnT-2, a mammalian protein that confers resistance to zinc by facilitating vesicular sequestration. EMBO J 1996;15:1784–1791
12. Kambe T, Narita H, Yamaguchi-Iwai Y, Hirose J, Amano T, Sugiura N, Sasaki R, Mori K, Iwanaga T, Nagao M. Cloning and characterization of a novel mammalian zinc transporter, zinc transporter 5, abundantly expressed in pancreatic β cells. J Biol Chem 2002;277:19049–19055
13. Cole TB, Wenzel HJ, Kafer KE, Schwartzkroin PA, Palmiter RD. Elimination of zinc from synaptic vesicles in the intact mouse brain by disruption of the ZnT3 gene. Proc Natl Acad Sci U S A 1999;96:1716–1721
14. Seve M, Chimienti F, Devergnas S, Favier A. In silico identification and expression of SLC30 family genes: an expressed sequence tag data mining strategy for the characterization of zinc transporters' tissue expression. BMC Genomics 2004;5:32
15. Wang Z, Li JY, Dahlstrom A, Danscher G. Zinc-enriched GABAergic terminals in mouse spinal cord. Brain Res 2001;921:165–172
16. Chimienti F, Devergnas S, Favier A, Seve M. Identification and cloning of a β-cell-specific zinc transporter, ZnT-8, localized into insulin secretory granules. Diabetes 2004;53:2330–2337
17. Chimienti F, Devergnas S, Pattou F, Schuit F, Garcia-Cuenca R, Vandewalle B, Kerr-Conte J, Van LL, Grunwald D, Favier A, Seve M. In vivo expression and functional characterization of the zinc transporter ZnT8 in glucose-induced insulin secretion. J Cell Sci 2006;119:4199–4206
18. Murgia C, Devirgiliis C, Mancini E, Donadel G, Zalewski P, Perozzi G. Diabetes-linked zinc transporter ZnT8 is a homodimeric protein expressed by distinct rodent endocrine cell types in the pancreas and other glands. Nutr Metab Cardiovasc Dis 2008 [Epub ahead of print]
19. Wenzlau JM, Juhl K, Yu L, Moua O, Sarkar SA, Gottlieb P, Rewers M, Eisenbarth GS, Jensen J, Davidson HW, Hutton JC. The cation efflux transporter ZnT8 (Slc30A8) is a major autoantigen in human type 1 diabetes. Proc Natl Acad Sci U S A 2007;104:17040–17045
20. Sladek R, Rocheleau G, Rung J, Dina C, Shen L, Serre D, Boutin P, Vincent D, Delisle A, Hadjadj S, Balkau B, Heude B, Charpentier G, Hundson TJ, Montpetit A, Pshezhetsky AV, Prentki M, Posner BI, Balding DJ, Meyre D, Polychronakos C, Froguel P. A genome-wide association study identifies novel risk loci for type 2 diabetes. Nature 2007;445:881–885
21. Frayling TM. Genome-wide association studies provide new insights into type 2 diabetes aetiology. Nat Rev Genet 2007;8:657–662
22. Steinthorsdottir V, Thorleifsson G, Reynisdottir I, Benediktsson R, Jonsdottir T, Walters GB, Styrkarsdottir U, Gretarsdottir S, Emilsson V, Ghosh S, Baker A, Snorradottir S, Bjarnason H, Ng MC, Hansen T, Bagger Y, Wilensky RL, Reilly MP, Adeyemo A, Chen Y, Zhou J, Gudnason V, Chen G, Huang H, Lashley K, Doumatey A, So WY, Ma RC, Andersen G, Borch-Johnsen K, Jorgensen T, van Vliet-Ostaptchouk JV, Hofker MH, Wijmenga C, Christiansen C, Rader DJ, Rotimi C, Gurney M, Chan JC, Pedersen O, Sigurdsson G, Gulcher JR, Thorsteinsdottir U, Kong A, Stefansson K. A variant in CDKAL1 influences insulin response and risk of type 2 diabetes. Nat Genet 2007;39:770–775
23. Kirchhoff K, Machicao F, Haupt A, Schafer SA, Tschritter O, Staiger H, Stefan N, Haring HU, Fritsche A. Polymorphisms in the TCF7L2, CDKAL1 and SLC30A8 genes are associated with impaired proinsulin conversion. Diabetologia 2008;51:597–601
24. da Silva Xavier G, Loder MK, McDonald A, Tarasov AI, Carzaniga R, Kronenberger K, Barg S, Rutter GA. TCF7L2 regulates late events in insulin secretion from pancreatic islet β-cells. Diabetes 2009;58:894–905
25. Castaing M, Duvillie B, Quemeneur E, Basmaciogullari A, Scharfmann R. Ex vivo analysis of acinar and endocrine cell development in the human embryonic pancreas. Dev Dyn 2005;234:339–345
26. Cross SE, Hughes SJ, Partridge CJ, Clark A, Gray DW, Johnson PR. Collagenase penetrates human pancreatic islets following standard intraductal administration. Transplantation 2008;86:907–911
27. Reimann F, Habib AM, Tolhurst G, Parker HE, Rogers GJ, Gribble FM. Glucose-sensing in L-cells: a primary cell study. Cell Metabolism 2008;8:532–539
28. da Silva Xavier G, Rutter J, Rutter GA. Involvement of Per-Arnt-Sim (PAS) kinase in the stimulation of preproinsulin and pancreatic duodenum homeobox 1 gene expression by glucose. Proc Natl Acad Sci U S A 2004;101:8319–8324
29. Burcelin R, Thorens B, Glauser M, Gaillard RC, Pralong FP. Gonadotropin-releasing hormone secretion from hypothalamic neurons: stimulation by insulin and potentiation by leptin. Endocrinology 2003;144:4484–4491
30. Cani PD, Knauf C, Iglesias MA, Drucker DJ, Delzenne NM, Burcelin R. Improvement of glucose tolerance and hepatic insulin sensitivity by oligofructose requires a functional glucagon-like peptide 1 receptor. Diabetes 2006;55:1484–1490
31. Cook S, Hugli O, Egli M, Vollenweider P, Burcelin R, Nicod P, Thorens B, Scherrer U. Clustering of cardiovascular risk factors mimicking the human metabolic syndrome X in eNOS null mice. Swiss Med Wkly 2003;133:360–363
32. He TC, Zhou S, da Costa LT, Yu J, Kinzler KW, Vogelstein B. A simplified system for generating recombinant adenoviruses. Proc Natl Acad Sci U S A 1998;95:2509–2514
33. Liu M, Li Y, Cavener D, Arvan P. Proinsulin disulfide maturation and misfolding in the endoplasmic reticulum. J Biol Chem 2005;280:13209–13212
34. Tarasov AI, Welters HJ, Senkel S, Ryffel GU, Hattersley AT, Morgan NG, Ashcroft FM. A Kir6.2 mutation causing neonatal diabetes impairs electrical activity and insulin secretion from INS-1 β-cells. Diabetes 2006;55:3075–3082
35. Tsuboi T, Rutter GA. Multiple forms of "kiss-and-run" exocytosis revealed by evanescent wave microscopy. Curr Biol 2003;13:563–567
36. Lu M, Fu D. Structure of the zinc transporter YiiP. Science 2007;317:1746–1748
37. Fiser A, Sali A. Modeller: generation and refinement of homology-based protein structure models. Methods Enzymol 2003;374:461–491
38. Haney CJ, Grass G, Franke S, Rensing C. New developments in the understanding of the cation diffusion facilitator family. J Ind Microbiol Biotechnol 2005;32:215–226
39. Berezin C, Glaser F, Rosenberg J, Paz I, Pupko T, Fariselli P, Casadio R, Ben-Tal N. ConSeq: the identification of functionally and structurally important residues in protein sequences. Bioinformatics 2004;20:1322–1324
40. Davis IW, Leaver-Fay A, Chen VB, Block JN, Kapral GJ, Wang X, Murray LW, Arendall WB III, Snoeyink J, Richardson JS, Richardson DC. MolProbity: all-atom contacts and structure validation for proteins and nucleic acids. Nucleic Acid Res 2007;35:W375–W383
41. Juhl K, Sarkar SA, Wong R, Jensen J, Hutton JC. Mouse pancreatic endocrine cell transcriptome defined in the embryonic Ngn3-null mouse. Diabetes 2008;57:2755–2761
42. Snitsarev V, Budde T, Stricker TP, Cox JM, Krupa DJ, Geng L, Kay AR. Fluorescent detection of Zn(2+)-rich vesicles with Zinquin: mechanism of action in lipid environments. Biophys J 2001;80:1538–1546
43. Wolters GH, Pasma A, Konijnendijk W, Boom G. Calcium, zinc and other elements in islet and exocrine tissue of the rat pancreas as measured by

histochemical methods and electron-probe micro-analysis, Effects of fasting and tolbutamide. Histochemistry 1979;62:1–17
44. Wan QF, Dong Y, Yang H, Lou X, Ding J, Xu T. Protein kinase activation increases insulin secretion by sensitizing the secretory machinery to Ca2+. J Gen Physiol 2004;124:653–662
45. Gyulkhandanyan AV, Lee SC, Bikopoulos G, Dai F, Wheeler MB. The Zn2+-transporting pathways in pancreatic β-cells: a role for the L-type voltage-gated Ca2+ channel. J Biol Chem 2006;281:9361–9372
46. Gyulkhandanyan AV, Lu H, Lee SC, Bhattacharjee A, Wijesekara N, Manning Fox JE, MacDonald PE, Chimienti F, Dai FF, Wheeler MB. Investigation of transport mechanisms and regulation of intracellular Zn2+ in pancreatic α-cells. J Biol Chem 2008;283:10184–10197
47. Ho LH, Ruffin RE, Murgia C, Li L, Krilis SA, Zalewski PD. Labile zinc and zinc transporter ZnT4 in mast cell granules: role in regulation of caspase activation and NF-κB translocation. J Immunol 2004;172:7750–7760
48. Zeggini E, Weedon MN, Lindgren CM, Frayling TM, Elliott KS, Lango H, Timpson NJ, Perry JR, Rayner NW, Freathy RM, Barrett JC, Shields B, Morris AP, Ellard S, Groves CJ, Harries LW, Marchini JL, Owen KR, Knight B, Cardon LR, Walker M, Hitman GA, Morris AD, Doney AS, McCarthy MI, Hattersley AT. Replication of Genome-Wide Association signals in U.K. Samples reveals risk loci for type 2 diabetes. Science 2007;316:1336–1341
49. Valentine RA, Jackson KA, Christie GR, Mathers JC, Taylor PM, Ford D. ZnT5 variant B is a bidirectional zinc transporter and mediates zinc uptake in human intestinal Caco-2 cells. J Biol Chem 2007;282:14389–14393
50. Cherezov V, Hofer N, Szebenyi DM, Kolaj O, Wall JG, Gillilan R, Srinivasan V, Jaroniec CP, Caffrey M. Insights into the mode of action of a putative zinc transporter CzrB in Thermus thermophilus. Structure 2008;16:1378–1388